

The Biharmonic Approach for Unsteady Flow Past an Impulsively Started Circular Cylinder

Jiten C Kalita^{1,*} and Shuvam Sen²

¹ *Department of Mathematics, Indian Institute of Technology Guwahati, PIN 781039, India.*

² *Department of Mathematical Sciences, Tezpur University, PIN 784028, India.*

Received 20 April 2011; Accepted (in revised version) 12 December 2011

Available online 17 April 2012

Abstract. In this paper, a newly developed second order temporally and spatially accurate finite difference scheme for biharmonic semi linear equations has been employed in simulating the time evolution of viscous flows past an impulsively started circular cylinder for Reynolds number (Re) up to 9,500. The robustness of the scheme and the effectiveness of the formulation can be gauged by the fact that it very accurately captures complex flow structures such as the von Kármán vortex street through streakline simulation and the α and β -phenomena in the range $3,000 \leq Re \leq 9,500$ among others. The main focus here is the application of the technique which enables the use of the discretized version of a single semi linear biharmonic equation in order to efficiently simulate different fluid structures associated with flows around a bluff body. We compare our results, both qualitatively and quantitatively, with established numerical and more so with experimental results. Excellent comparison is obtained in all the cases.

AMS subject classifications: 35Q30, 65M06, 76D05, 76D25

Key words: Biharmonic, non-rectangular, N-S equations, transient, circular cylinder, von Kármán vortex street.

1 Introduction

Flow over a bluff body is a common phenomenon which occurs when fluid flows over an obstacle or along with the movement of a natural or artificial body. Common examples are the flows past an airplane, a submarine, an automobile, or wind blowing past a high-rise building. Although bluff bodies exist in many different shapes, the circular cylinder is considered to be the representative of a two dimensional bluff body. As such, the flow

*Corresponding author. *Email addresses:* jiten@iitg.ernet.in (J. C. Kalita), shuvam@tezu.ernet.in (S. Sen)

around a circular cylinder has been the subject of intense research in the last century and numerous theoretical, numerical and experimental investigations have been reported in the literature [1–18]. The time development of an incompressible viscous flow induced by an impulsively started circular cylinder is now a classical problem in fluid mechanics. It displays almost all the fluid mechanical phenomena for incompressible viscous flows in the simplest of geometric settings.

In the context of numerical studies on this problem, with the advent of Computational Fluid Dynamics (CFD), more and more computational methods for simulating fluid flows are coming into the fore [10–16, 19–25] which has led to the better understanding of the characteristics of the flow. Numerical simulation could now invade areas hitherto unexplored by experimentalists where it is possible to analyze all aspects of the flow at each stage of its development. A quick look at these works reveals that there exists only a few studies where a single numerical scheme has been employed to tackle the flow throughout the whole range of $10^0 \leq Re \leq 10^4$. The ranges of Reynolds numbers which came under the purview of these works, varied from one study to the other. Although investigations on vortex shedding has been quite popular with the experimentalists ever since Roshko [6] first measured the period of von Kármán vortex shedding behind a bluff body, the simulation and characteristic study of streak lines seem to have failed to attract the attention of numerical analysts. One of the objectives of the present study is also to address these two issues apart from capturing other flow characteristics for this problem.

Fluid flow problems governed by Navier-Stokes (N-S) equations can be solved by using a variety of numerical methods. As is well established, these methods can broadly be classified as finite difference, finite volume or finite element approach. Amongst these, finite difference (FD) method is the most popular approach that has been used quite frequently in CFD because of its easiness in implementation. In the FD set up, approximation of a higher order derivative generally requires more points and as such is associated with non-compact stencils. Such schemes, which are used for higher order differential equations on non-compact stencils, require additional conditions in order to tackle the difficulty of flow computation at the boundary. Contrary to these, a compact finite difference scheme [26–28] which utilizes grid points located only directly adjacent to the node, computes the flow with information solely from the nearest neighbours and are gaining popularity *via-a-vis* wide-molecule schemes [29–32].

Over the years, the CFD community has seen the extensive use of both the primitive variable and stream function-vorticity (ψ - ω) formulation to compute incompressible viscous flows governed by the N-S equations. Both these formulations have their relative advantages and disadvantages over each other: while the primitive variable formulation has been traditionally difficult because of the presence of the pressure term in the governing equations, a typical difficulty with the ψ - ω formulation is that the vorticity ω is not prescribed on the boundaries. Due to these facts, the biharmonic pure stream function form of the N-S equations, which eliminates the need to compute both pressure and vorticity, is emerging as an attractive alternative [33–36]. Besides, this approach has the advantage of requiring to solve only a single fourth order PDE instead of a system of

second order PDEs.

However, the schemes developed so far for the biharmonic pure stream function form of the N-S equations were capable of computing the flow only for simple rectangular geometries on uniform grids. Efficient implementation of the velocity-stream function approach spearheaded by Gupta and Kalita [35,36] in its original form is extremely difficult, if not impossible on nonrectangular physical domains. In the present study, we use a newly proposed [37] compact second order temporally and spatially accurate FD scheme for the biharmonic pure stream function form of transient N-S equations on non-uniform grids which is capable of tackling geometries beyond rectangular and hence can be used to simulate the dynamics of fully coupled flow-body system. We chose the problem of impulsively started circular cylinder because of the availability of benchmark experimental as well as numerical results and therefore serve very well as a suitable test case for accuracy and effectiveness of the newly proposed technique. The grid is constructed using a conformal mapping, which results in a general orthogonal grid, where the degree and nature of the non-uniformity can be specified to meet the needs of the problem being studied. The added advantage of our approach is that no other boundary condition is required except for stream function and velocity. To the best of our knowledge this is the first attempt to simulate flow around a bluff body by using a single discretized equation instead of a system of equations.

Our main focus in this paper is to analyze the flow past an impulsively started circular cylinder in different laminar flow regimes using a single numerical scheme and compare our numerical results with established experimental and numerical ones. Time evolution of flow structure is studied through numerical simulation for a wide range of Reynolds numbers ranging from 50 to 9,500. This includes the visualization of the flow by numerically generating streak lines. The computations are performed by time marching, using a predictor-corrector approach. Despite being spatially lower order accurate than traditional higher order compact schemes, the numerical solutions obtained through the proposed scheme are in excellent match with the available experimental and established numerical results as would be seen later. This is due to the fact that the scheme utilizes the advantage of grid clustering in the regions of small scales which invariably requires more grid points to resolve the scale irrespective of the spatial accuracy of the scheme.

The paper has been arranged in six sections. Section 2 deals with the mathematical formulation and discretization procedures, Section 3 with the problem and the numerical issues, Section 4 with the solution of the algebraic system of equations, Section 5 with the numerical results and finally, Section 6 summarizes the whole work.

2 Mathematical formulations and discretization procedures

2.1 Mathematical formulation

The unsteady 2D incompressible viscous flows are governed by the N-S equations. In cartesian (x,y) coordinate system, the non-dimensional form of these equations can be

written as:

$$\frac{\partial u}{\partial x} + \frac{\partial v}{\partial y} = 0, \quad (2.1)$$

$$\frac{1}{2} \frac{\partial u}{\partial t} + u \frac{\partial u}{\partial x} + v \frac{\partial u}{\partial y} = -\frac{\partial p}{\partial x} + \frac{2}{Re} \left(\frac{\partial^2 u}{\partial x^2} + \frac{\partial^2 u}{\partial y^2} \right), \quad (2.2)$$

$$\frac{1}{2} \frac{\partial v}{\partial t} + u \frac{\partial v}{\partial x} + v \frac{\partial v}{\partial y} = -\frac{\partial p}{\partial y} + \frac{2}{Re} \left(\frac{\partial^2 v}{\partial x^2} + \frac{\partial^2 v}{\partial y^2} \right). \quad (2.3)$$

Here u, v are non-dimensional velocities along x, y -directions respectively and p is the pressure. The Reynolds number Re is defined as $Re = DU_\infty/\nu$ where $D = 2a$ is the diameter of the cylinder, U_∞ is the free-stream velocity and ν kinematic viscosity. The non-dimensionalization have been carried out following [38]. Introducing stream function ψ and vorticity ω we have

$$u = \frac{\partial \psi}{\partial y}, \quad v = -\frac{\partial \psi}{\partial x}, \quad \omega = \frac{\partial v}{\partial x} - \frac{\partial u}{\partial y}$$

and the above formulation may be rewritten as:

$$\frac{\partial^2 \psi}{\partial x^2} + \frac{\partial^2 \psi}{\partial y^2} = -\omega, \quad (2.4)$$

$$\frac{1}{2} \frac{\partial \omega}{\partial t} = \frac{2}{Re} \left(\frac{\partial^2 \omega}{\partial x^2} + \frac{\partial^2 \omega}{\partial y^2} \right) - \left(u \frac{\partial \omega}{\partial x} + v \frac{\partial \omega}{\partial y} \right). \quad (2.5)$$

As is well known a rectangular grid on an irregular physical domain needs special treatment. To circumvent this we take help of coordinate transformation and convert a non-rectangular physical domain onto a rectangular computational domain. Let the physical (x, y) plane be transformed into a computational (ξ, η) plane using the mapping:

$$x = x(\xi, \eta), \quad y = y(\xi, \eta). \quad (2.6)$$

Under this transformation Eqs. (2.4) and (2.5) in the computational plane becomes:

$$a_1 \frac{\partial^2 \psi}{\partial \xi^2} + e_1 \frac{\partial^2 \psi}{\partial \xi \partial \eta} + b_1 \frac{\partial^2 \psi}{\partial \eta^2} + c_1 \frac{\partial \psi}{\partial \xi} + d_1 \frac{\partial \psi}{\partial \eta} = f_1, \quad (2.7)$$

$$\frac{1}{2} \frac{\partial \omega}{\partial t} = a_2 \frac{\partial^2 \omega}{\partial \xi^2} + e_2 \frac{\partial^2 \omega}{\partial \xi \partial \eta} + b_2 \frac{\partial^2 \omega}{\partial \eta^2} + c_2 \frac{\partial \omega}{\partial \xi} + d_2 \frac{\partial \omega}{\partial \eta}, \quad (2.8)$$

where

$$a_1 = \frac{1}{J^2} (x_\eta^2 + y_\eta^2), \quad b_1 = \frac{1}{J^2} (x_\xi^2 + y_\xi^2),$$

$$c_1 = \frac{1}{J^3} \left[-y_\eta ((x_\eta^2 + y_\eta^2) x_{\xi\xi} - 2(y_\eta y_\xi + x_\eta x_\xi) x_{\xi\eta} + (x_\xi^2 + y_\xi^2) x_{\eta\eta}) \right. \\ \left. + x_\eta ((x_\eta^2 + y_\eta^2) y_{\xi\xi} - 2(y_\eta y_\xi + x_\eta x_\xi) y_{\xi\eta} + (x_\xi^2 + y_\xi^2) y_{\eta\eta}) \right],$$

$$\begin{aligned}
 d_1 &= \frac{1}{J^3} \left[y_\xi ((x_\eta^2 + y_\eta^2) x_{\xi\xi} - 2(y_\eta y_\xi + x_\eta x_\xi) x_{\xi\eta} + (x_\xi^2 + y_\xi^2) x_{\eta\eta}) \right. \\
 &\quad \left. - x_\xi ((x_\eta^2 + y_\eta^2) y_{\xi\xi} - 2(y_\eta y_\xi + x_\eta x_\xi) y_{\xi\eta} + (x_\xi^2 + y_\xi^2) y_{\eta\eta}) \right], \\
 e_1 &= -\frac{2}{J^2} (y_\eta y_\xi + x_\eta x_\xi), \quad f_1 = -\omega, \\
 a_2 &= \frac{2}{ReJ^2} (x_\eta^2 + y_\eta^2), \quad b_2 = \frac{2}{ReJ^2} (x_\xi^2 + y_\xi^2), \\
 c_2 &= \frac{1}{J} (u y_\eta - v x_\eta) + \frac{2}{ReJ^3} \left[-y_\eta ((x_\eta^2 + y_\eta^2) x_{\xi\xi} - 2(y_\eta y_\xi + x_\eta x_\xi) x_{\xi\eta} + (x_\xi^2 + y_\xi^2) x_{\eta\eta}) \right. \\
 &\quad \left. + x_\eta ((x_\eta^2 + y_\eta^2) y_{\xi\xi} - 2(y_\eta y_\xi + x_\eta x_\xi) y_{\xi\eta} + (x_\xi^2 + y_\xi^2) y_{\eta\eta}) \right], \\
 d_2 &= \frac{1}{J} (-u y_\xi + v x_\xi) + \frac{2}{ReJ^3} \left[y_\xi ((x_\eta^2 + y_\eta^2) x_{\xi\xi} - 2(y_\eta y_\xi + x_\eta x_\xi) x_{\xi\eta} + (x_\xi^2 + y_\xi^2) x_{\eta\eta}) \right. \\
 &\quad \left. - x_\xi ((x_\eta^2 + y_\eta^2) y_{\xi\xi} - 2(y_\eta y_\xi + x_\eta x_\xi) y_{\xi\eta} + (x_\xi^2 + y_\xi^2) y_{\eta\eta}) \right], \\
 e_2 &= -\frac{4}{ReJ^2} (y_\eta y_\xi + x_\eta x_\xi),
 \end{aligned}$$

where $J = x_\xi y_\eta - y_\xi x_\eta$ is the Jacobian of the transformation with

$$u = \frac{1}{J} \left(\frac{\partial \psi}{\partial \eta} x_\xi - \frac{\partial \psi}{\partial \xi} x_\eta \right), \tag{2.9}$$

$$v = \frac{1}{J} \left(-\frac{\partial \psi}{\partial \xi} y_\eta + \frac{\partial \psi}{\partial \eta} y_\xi \right). \tag{2.10}$$

If the transformation (2.6) is a conformal transformation i.e. of the form:

$$z = z(\theta), \tag{2.11}$$

$z = x + iy$ and $\theta = \xi + i\eta$ then Eqs. (2.7) and (2.8) simplify to:

$$\frac{1}{J} \left(\frac{\partial^2 \psi}{\partial \xi^2} + \frac{\partial^2 \psi}{\partial \eta^2} \right) = -\omega, \tag{2.12}$$

$$\frac{1}{2} \frac{\partial \omega}{\partial t} = \frac{2}{ReJ} \left(\frac{\partial^2 \omega}{\partial \xi^2} + \frac{\partial^2 \omega}{\partial \eta^2} \right) - \frac{1}{J} \left(\frac{\partial \omega}{\partial \xi} \frac{\partial \psi}{\partial \eta} - \frac{\partial \omega}{\partial \eta} \frac{\partial \psi}{\partial \xi} \right). \tag{2.13}$$

In deriving Eq. (2.13) expressions (2.9) and (2.10) have also been made use of. Note that in this case the Jacobian of the transformation is, $J = x_\xi y_\eta - y_\xi x_\eta = x_\xi^2 + y_\xi^2 = x_\eta^2 + y_\eta^2$.

Eliminating ω from Eqs. (2.12) and (2.13), we obtain the following form of the N-S

equations:

$$\begin{aligned} & \frac{ReJ}{4} \frac{\partial}{\partial t} \left(\frac{\partial^2 \psi}{\partial \xi^2} + \frac{\partial^2 \psi}{\partial \eta^2} \right) \\ &= \left(\frac{\partial^4 \psi}{\partial \xi^4} + 2 \frac{\partial^4 \psi}{\partial \xi^2 \partial \eta^2} + \frac{\partial^4 \psi}{\partial \eta^4} \right) - \left(2C + \frac{Re}{2} \frac{\partial \psi}{\partial \eta} \right) \left(\frac{\partial^3 \psi}{\partial \xi^3} + \frac{\partial^3 \psi}{\partial \xi \partial \eta^2} \right) \\ & \quad - \left(2D - \frac{Re}{2} \frac{\partial \psi}{\partial \xi} \right) \left(\frac{\partial^3 \psi}{\partial \xi^2 \partial \eta} + \frac{\partial^3 \psi}{\partial \eta^3} \right) + \left(E + C \frac{Re}{2} \frac{\partial \psi}{\partial \eta} - D \frac{Re}{2} \frac{\partial \psi}{\partial \xi} \right) \left(\frac{\partial^2 \psi}{\partial \xi^2} + \frac{\partial^2 \psi}{\partial \eta^2} \right), \end{aligned} \tag{2.14}$$

where $C = J_{\xi} / J$, $D = J_{\eta} / J$, and $E = 2C^2 + 2D^2 - J_{\eta\eta} / J - J_{\xi\xi} / J$. This is a fourth order transient semi-linear partial differential equation.

Eq. (2.14) is of form

$$\frac{\partial}{\partial t} \Delta \psi = a(\xi, \eta) \Delta^2 \psi + b(\xi, \eta, \psi_{\xi}, \psi_{\eta}) \Delta \psi_{\xi} + c(\xi, \eta, \psi_{\xi}, \psi_{\eta}) \Delta \psi_{\eta} + d(\xi, \eta, \psi_{\xi}, \psi_{\eta}) \Delta \psi \tag{2.15}$$

with $a(\xi, \eta) > 0$ and can be termed as the biharmonic form of the N-S equation in the transformed plane. It contains ψ as the only dependent variable from which other flow variables can be post processed in contrast to the other cases *viz.* (A) three dependent variables u, v , and p associated with the system of equations (2.1) to (2.3) and (B) two dependent variable ψ and ω associated with the system of equations (2.4) and (2.5). Hence Eq. (2.14) is much more handy for numerical simulation.

2.2 Discretization

The spatial operators $\Delta_h^2 \psi_{i,j}$ and $\Delta_h \psi_{i,j}$ present in Eq. (2.15) are discretized as:

$$\begin{aligned} \Delta_h^2 \psi_{i,j} = & \frac{2}{h^4} \left(28\psi_{i,j} - 8(\psi_{i+1,j} + \psi_{i,j+1} + \psi_{i-1,j} + \psi_{i,j-1}) \right. \\ & \quad \left. + (\psi_{i+1,j+1} + \psi_{i-1,j+1} + \psi_{i+1,j-1} + \psi_{i-1,j-1}) \right. \\ & \quad \left. + 3h(\psi_{\xi_{i+1,j}} - \psi_{\xi_{i-1,j}} + \psi_{\eta_{i,j+1}} - \psi_{\eta_{i,j-1}}) \right) + \mathcal{O}(h^2), \end{aligned} \tag{2.16}$$

$$\Delta_h \psi_{i,j} = \frac{1}{h^2} \left(\psi_{i+1,j} + \psi_{i,j+1} - 4\psi_{i,j} + \psi_{i-1,j} + \psi_{i,j-1} \right) + \mathcal{O}(h^2). \tag{2.17}$$

Since (2.16) carries ψ_{ξ} and ψ_{η} they need to be approximated compactly and are given as:

$$\psi_{\xi_{i+1,j}} + 4\psi_{\xi_{i,j}} + \psi_{\xi_{i-1,j}} = \frac{3}{h} (\psi_{i+1,j} - \psi_{i-1,j}) + \mathcal{O}(h^4), \tag{2.18}$$

$$\psi_{\eta_{i,j+1}} + 4\psi_{\eta_{i,j}} + \psi_{\eta_{i,j-1}} = \frac{3}{h} (\psi_{i,j+1} - \psi_{i,j-1}) + \mathcal{O}(h^4). \tag{2.19}$$

The time derivative has been discretized by a Crank-Nicolson type of approximation to obtain a finite difference scheme for equation (2.15) as:

$$\Delta_h \psi_{i,j}^{(n+1)} = \Delta_h \psi_{i,j}^{(n)} + \delta t (1 - \lambda) \left[a_{i,j} \Delta_h^2 \psi_{i,j}^{(n)} + b_{i,j} \Delta_h \psi_{\xi_{i,j}}^{(n)} + c_{i,j} \Delta_h \psi_{\eta_{i,j}}^{(n)} + d_{i,j} \Delta_h \psi_{i,j}^{(n)} \right] + \delta t \lambda \left[a_{i,j} \Delta_h^2 \psi_{i,j}^{(n+1)} + b_{i,j} \Delta_h \psi_{\xi_{i,j}}^{(n+1)} + c_{i,j} \Delta_h \psi_{\eta_{i,j}}^{(n+1)} + d_{i,j} \Delta_h \psi_{i,j}^{(n+1)} \right]. \quad (2.20)$$

With $\lambda = \frac{1}{2}$ Eq. (2.20) yields an $\mathcal{O}(h^2; \delta t^2)$ accurate scheme.

3 The problem and the numerical issues

The schematic diagram is presented in Fig. 1(a). The cylinder is considered to be of unit radius with uniform free-stream velocity $U_\infty = 1$ and far-field $R_\infty \approx 43$. A typical computational grid of size 61×101 are shown in Fig. 1(b). We employ a uniform grid spacing along the cross radial direction and nonuniform grid spacing in the radial direction with

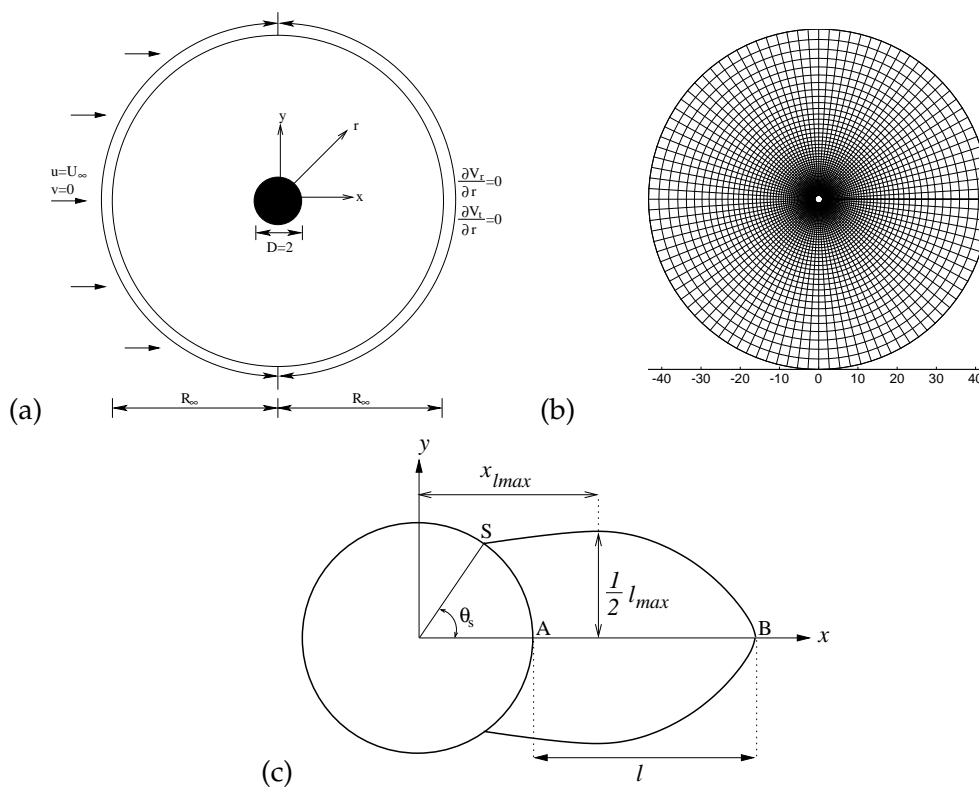


Figure 1: (a) Configuration of the flow past a circular cylinder problem; (b) A typical 61×101 grid; (c) Geometrical parameters of the closed wake for the motion past a circular cylinder.

clustering around the surface of the cylinder so that propagation of large solution error can be avoided [39]. The conformal transformation considered here is

$$x = e^{(\pi\xi)} \cos(\pi\eta), \quad y = e^{(\pi\xi)} \sin(\pi\eta).$$

Under this transformation Eq. (2.14) reduces to

$$Re \frac{\pi^2 e^{2\pi\xi}}{4} \frac{\partial}{\partial t} \Delta\psi = \Delta^2\psi - \left(4\pi + \frac{Re}{2} \psi_\eta\right) \Delta\psi_\xi + \frac{Re}{2} \psi_\xi \Delta\psi_\eta + 2\pi \left(2\pi + \frac{Re}{2} \psi_\eta\right) \Delta\psi. \quad (3.1)$$

Using (2.20), an implicit $\mathcal{O}(h^2; \delta t^2)$ accurate finite difference approximation for (3.1) is obtained as:

$$\begin{aligned} Re \frac{\pi^2 e^{2\pi\xi_i}}{4} \Delta_h \psi_{i,j}^{(n+1)} = & Re \frac{\pi^2 e^{2\pi\xi_i}}{4} \Delta_h \psi_{i,j}^{(n)} + (1-\lambda)\delta t \left[\Delta_h^2 \psi_{i,j}^{(n)} - \left(4\pi + \frac{Re}{2} \psi_{\eta_{i,j}}^{(n)}\right) \Delta_h \psi_{\xi_{i,j}}^{(n)} \right. \\ & \left. + \frac{Re}{2} \psi_{\xi_{i,j}}^{(n)} \Delta_h \psi_{\xi_{i,j}}^{(n)} + 2\pi \left(2\pi + \frac{Re}{2} \psi_{\eta_{i,j}}^{(n)}\right) \Delta_h \psi_{i,j}^{(n)} \right] \\ & + \lambda\delta t \left[\Delta_h^2 \psi_{i,j}^{(n+1)} - \left(4\pi + \frac{Re}{2} \psi_{\eta_{i,j}}^{(n+1)}\right) \Delta_h \psi_{\xi_{i,j}}^{(n+1)} \right. \\ & \left. + \frac{Re}{2} \psi_{\xi_{i,j}}^{(n+1)} \Delta_h \psi_{\xi_{i,j}}^{(n+1)} + 2\pi \left(2\pi + \frac{Re}{2} \psi_{\eta_{i,j}}^{(n+1)}\right) \Delta_h \psi_{i,j}^{(n+1)} \right]. \quad (3.2) \end{aligned}$$

We estimate the boundary conditions for stream function and its first order derivatives as below:

1. On the surface of the cylinder $\xi = 0, u = v = 0 \Rightarrow \psi_\xi = 0, \psi_\eta = 0, \psi = 0$.
2. In the far upstream $u = U_\infty, v = 0 \Rightarrow \psi_\xi = \pi e^{(\pi\xi)} \sin(\pi\eta), \psi_\eta = \pi e^{(\pi\xi)} \cos(\pi\eta)$ and $\psi = e^{(\pi\xi)} \sin(\pi\eta)$ which corresponds to the potential flow.
3. In the far downstream we use the Neumann condition that $\frac{\partial V_i}{\partial \xi} = 0 = \frac{\partial V_i}{\partial \xi}$. One sided second order approximation translates these conditions to,

$$\psi_{\eta_{imax,j}} \doteq \frac{1}{3} (4e^{\pi h} \psi_{\eta_{imax-1,j}} - e^{2\pi h} \psi_{\eta_{imax-2,j}}), \quad \psi_{\xi_{imax,j}} \doteq \frac{1}{3} (4e^{\pi h} \psi_{\xi_{imax-1,j}} - e^{2\pi h} \psi_{\xi_{imax-2,j}}),$$

respectively.

It should be noted here that once the vortex shedding starts, at the downstream of the flow, one needs to use convective boundary condition for ψ , i.e. $\frac{\partial \psi}{\partial t} + U_\infty \frac{\partial \psi}{\partial x} = 0$. For such flows, where aim is to simulate vortex shedding, at the downstream of the flow, potential boundary condition for ψ has been replaced by convective boundary condition and was found to be quite efficient. Again for flows with higher Re the convective boundary condition at the very initial stage of flow does not work well. Thus if one wishes to simulate a flow from very beginning to the final vortex shedding state an ideal choice

will be to march first few iterations say till non dimensional time 0.25 with the potential boundary condition and then to proceed with the convective boundary condition. As far as the initial condition is concerned we have started with $\psi = 0$ everywhere except at the boundary as also $\psi_\xi = \psi_\eta = 0$ everywhere except at the upstream boundary. Note that the implicitness of Eq. (3.2) allows our scheme to use larger time step, and it is seen that a value of δt as large as 0.01 is sufficient to carry out a stable computation. However, in order to accurately capture the time evolution of the flow, we use $\delta t = 0.001$ for all the simulations considered in this work.

4 The solution of algebraic system of equations

Let us now discuss the solution of algebraic systems associated with the finite difference approximation (3.2). As we are interested in second order accuracy in time we chose $\lambda = \frac{1}{2}$. The resulting system of equation in matrix form can be written as:

$$A_1 \Psi^{(n+1)} = F_1 \left(\Psi^{(n)}, \Psi_\xi^{(n)}, \Psi_\eta^{(n)}, \Psi_\xi^{(n+1)}, \Psi_\eta^{(n+1)} \right). \tag{4.1}$$

For a grid of size $m \times n$, the matrix A_1 has the dimension mn . Due to the compact nature of our scheme A_1 is a banded matrix with nine non zero diagonals. Also $\Psi^{(n+1)}, \Psi^{(n)}, \Psi_\xi^{(n)}, \Psi_\eta^{(n)}, \Psi_\xi^{(n+1)}, \Psi_\eta^{(n+1)}$ are all mn component vectors. At any time step once $\Psi^{(n)}$ has been approximated $\Psi_\xi^{(n)}, \Psi_\eta^{(n)}$ can be obtained by solving tridiagonal systems

$$A_2 \Psi_\xi^{(n)} = F_2(\Psi^{(n)}), \tag{4.2}$$

$$A_3 \Psi_\eta^{(n)} = F_3(\Psi^{(n)}), \tag{4.3}$$

respectively. Eqs. (4.2) and (4.3) are the corresponding matrix forms of the relations (2.18) and (2.19). Thus the main objective now is to solve Eq. (4.1), thereby evaluating unknown vector $\Psi^{(n+1)}$. But a difficulty arises due the presence of $(n+1)$ th time level gradients of Ψ on the right hand side of Eq. (4.1) as those quantities will be available only after solving for stream function at the $(n+1)$ th time level. To overcome this difficulty we adopt a predictor-corrector approach. By setting $\lambda = 0$ in Eq. (3.2) we get a first order time accurate formula which has the matrix representation

$$A_4 \Psi^{(n+1)} = F_4 \left(\Psi^{(n)}, \Psi_\xi^{(n)}, \Psi_\eta^{(n)} \right). \tag{4.4}$$

Here A_4 is a matrix with only five non zero diagonals and we have the advantage that $\Psi^{(n+1)}$ can be estimated directly.

Direct solution of any of the above linear system is impractical because of huge size of the coefficient matrix and enormous storage requirements even for moderate values of step size h . On the other hand condition number of the coefficient matrix increases rapidly with reduced step size h and one must be very cautious when attempting to solve

such linear systems using iterative solvers. As the coefficient matrix A_1 is not diagonally dominant, conventional solvers such as Gauss-Seidel also cannot be used. Therefore all the computations were performed using the biconjugate gradient stabilized (BiCGStab) [40] method without preconditioning, where, thanks to the compact grid, it is easy to implement matrix vector multiplication $A_1\Psi$ without the need of storing all the entries of the matrix A_1 . It is worth mentioning here that in solving all the linear systems mentioned above nowhere we felt the need to under relax or over relax any of the parameters. This is indeed a refreshing experience as compared to solving formulations based of vorticity-stream function or primitive variable where there is a severe need to under relax quite a few parameters.

The convergence criterion for BiCGStab iteration based on norm of residual was set at 10^{-8} and the stopping criterion for the corrector was set at 10^{-12} . All our computations were carried out on a Pentium Dual-Core processor based PC with 2 GB RAM using double precision floating point arithmetic.

5 Numerical results

The drag D on the surface of a cylinder of radius r is $D = \rho r U_\infty^2 C_D$, where C_D is a non-dimensional coefficient. Following [41], the formula for evaluating C_D on the surface of a cylinder of radius r can be written as:

$$C_D = \frac{1}{2\pi r} \int_0^2 \{ (\psi_\xi^2 - \psi_\eta^2) \cos(\pi\eta) - \psi_\xi \psi_\eta \sin(\pi\eta) \} d\eta - r \int_0^2 \psi_\eta \omega \sin(\pi\eta) d\eta + \frac{2r}{Re} \int_0^2 (\omega_\xi - \pi\omega) \sin(\pi\eta) d\eta. \quad (5.1)$$

Using the expression for ω that can be obtained from Eq. (2.7) and the boundary conditions on the surface of the cylinder the above formula for $r=1$ can be simplified to:

$$C_D = \frac{2}{\pi^2 Re} \int_0^2 (3\pi\psi_{\xi\xi} - \psi_{\xi\xi\xi}) \sin(\pi\eta) d\eta.$$

Similarly the expression for lift coefficient becomes:

$$C_L = \frac{2}{\pi^2 Re} \int_0^2 (3\pi\psi_{\xi\xi} - \psi_{\xi\xi\xi}) \cos(\pi\eta) d\eta.$$

This enables us to describe the entire problem purely in terms of stream function. The above integrals has been evaluated by using Simpson's one-third formula.

We intend to use the formulation developed here to numerically simulate and compare experimental results available in literature. This can be used to further our understanding of flow past impulsively started circular cylinder.

As it is well established by now that immediately after the fluid motion starts, the flow is irrotational everywhere. But gradually, due to the fluid motion vorticity is generated

on the surface of the cylinder and slowly it is transported to the rear stagnation point and flow reversal takes place. After a short period of time for flows with $Re > 5$ a recirculating zone appears and it continues to grow eventually leading to the flow separation. The time development of flow differs with Re increasing. In order to establish the robustness of the scheme we focus our attention in the Re range of 50 to 9,500. In the first part we discuss about the flow structures for $50 \leq Re \leq 550$ where the wake behind the cylinder becomes unstable as time progresses. Oscillations in the wake grow in amplitude and finally forms a trail of vortices known as von Kármán vortex street. Next we consider the laminar regime in the Reynolds number range $3,000 \leq Re \leq 9,500$ in the early stages after the impulsive start. In this part flow is characterized by the most complicated structures associated with the α - and β -phenomena. We carry out our computation with a value of $R_\infty \approx 43$ on a grid of size 181×301 .

5.1 Flows for $50 \leq Re \leq 550$

The flow around a impulsively started circular cylinder for this range eventually becomes periodic and is known to develop vortex shedding represented by the von Kármán vortex street. As the flow starts impulsively, a recirculating eddy quickly develops behind the cylinder and evolves with time. We tabulate the evolution of the maximum width l_{max} and the abscissa of this maximum $x_{l_{max}}$, as defined in Fig. 1(c), of the recirculating zone for $Re = 200$ and 550 in Table 1. In this table we also compare our numerical results with the experimental ones given by Bouard and Coutanceau [38]. A good comparison can be seen in this table. Further for $Re = 550$ we compare velocity distribution on flow axis at early times with the experimental work [38]. Again a very good comparison can be seen.

During the development of the periodic vortex shedding, the flow goes through different phases eventually leading to the development of so called von Kármán vortex

Table 1: Comparison of numerical values of the magnitude and of the abscissa of the maximum width for various Re and t with experimental observations [38] (value shown with parenthesis).

t		1	1.5	2.0	2.5	3.0
$Re = 200$	$x_{l_{max}}/D$	0.37 (0.35)	0.52 (0.51)	0.66 (0.65)	0.77 (0.76)	0.85 (0.86)
	l_{max}/D	0.92 (0.94)	0.99 (0.97)	1.05 (1.02)	1.10 (1.07)	1.15 (1.10)
$Re = 550$	$x_{l_{max}}/D$	0.26 (0.30)	0.43 (0.50)	0.65 (0.66)	0.73 (0.76)	0.80 (0.85)
	l_{max}/D	0.95 (0.94)	1.00 (0.98)	1.05 (1.03)	1.12 (1.10)	1.18 (1.16)
$Re = 3,000$	$x_{l_{max}}/D$	0.16 (0.19)	0.27 (0.26)	0.36 (0.40)	0.67 (0.73)	0.80 (0.84)
	l_{max}/D	0.98 (0.93)	1.02 (0.98)	1.08 (1.04)	1.14 (1.11)	1.20 (1.20)

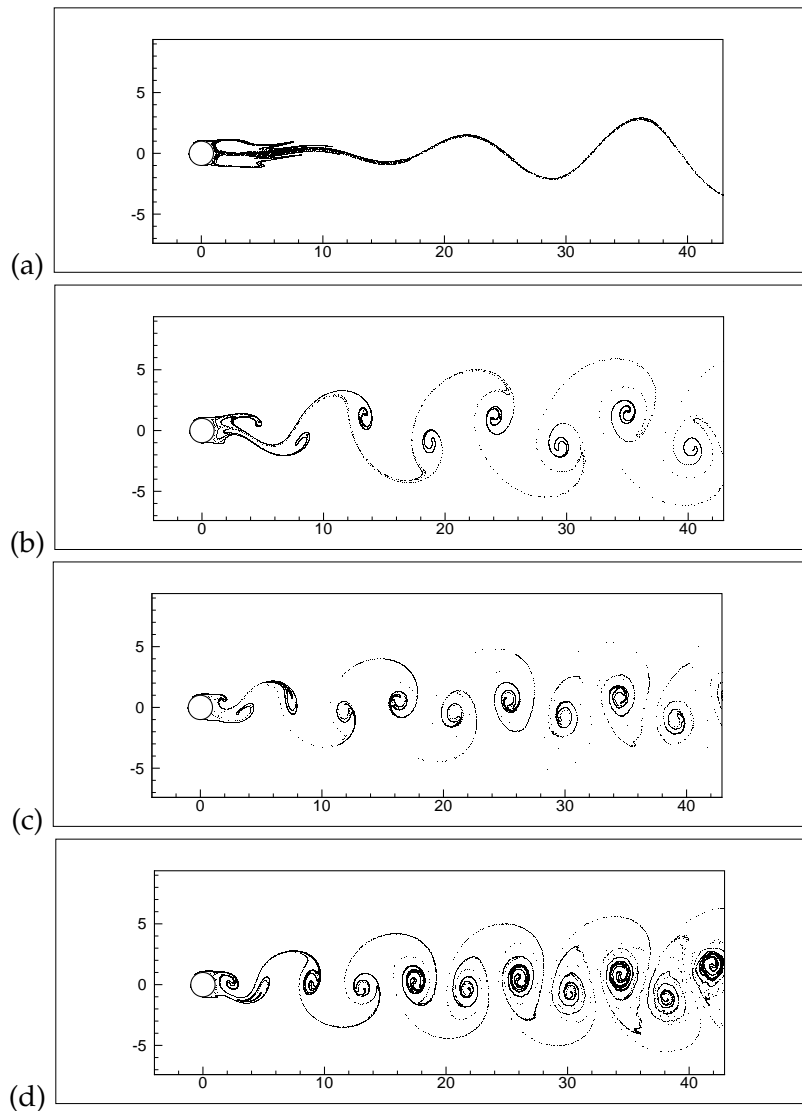


Figure 2: Streak lines for (a) $Re = 50$, (b) $Re = 100$, (c) $Re = 200$, (d) $Re = 300$.

street. Once shedding has been initiated, the vortices are shed in a routine manner alternately from the two sides of the cylinder. As time progresses, shedding frequency increases until a limiting condition is reached. As the flow fully develops, both the drag and lift coefficients reach periodic nature. The characteristics of the final periodic state depends on Re under consideration. With the increase in Re value the shedding becomes more pronounced. In experimental setup this is clearly depicted by streak lines while in numerical simulation the phenomena is captured by estimation of Strouhal number. Streaklines are seldom shown in numerical computations. One of the objectives in this

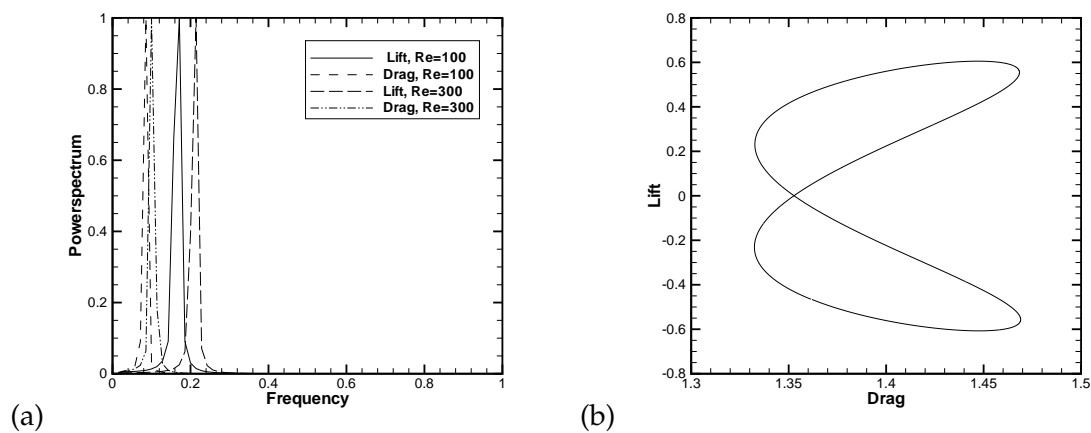


Figure 3: (a) Power spectrum of Drag and Lift coefficient for $Re=100$, $Re=300$; (b) Phase diagram of Drag and Lift coefficients for $Re=300$.

section of the present work is to examine the properties of the streakline patterns behind a circular cylinder during the process of vortex shedding. In incompressible flow, vorticity is generated only at solid boundaries, which, for this problem is the surface of the cylinder, and this vorticity resides within the fluid. The streaklines for $Re=50$, 100, 200, and 300 are presented in Fig. 2. These streaklines provide an effective view of the spots in the flow field where the vorticity is inherent. Our computed streakline patterns for the range of Reynolds numbers in these figures are in conjunction with those depicted in [18,42]. Note that the relationship between instantaneous streamlines and streaklines is extremely complex and visualization of both is necessary for proper understanding of flow field character. As is well known, our numerical streaklines remain continuous without breakage although they get thinned up. Streaklines now represent a flexible barrier which a fluid can never cross, and is quite evident from the Fig. 2(a)-(d). The fluid entering the wake moves in and jumps towards the cylinder surface in turn from both sides and are eventually squeezed out of the wake and roll-up. The two sets of vortex sheets intertwine with each other in the far wake and this have been completely captured by our simulation.

We also calculate the Strouhal St number which characterizes the vortex shedding process and is estimated from the periodic variation of the lift coefficient. It is defined as $St = \frac{nD}{U_\infty}$, where n is the dominant frequency of the lift variations, which we compute by a spectral analysis of a time sample of the lift coefficients. The power density spectra of this analysis normalized by the maximum value for $Re=100$ and $Re=300$ is shown in Fig. 3(a); Fig. 3(b) displays the phase-plane of the drag and lift coefficients for the same time sample for $Re=300$; it clearly establishes that the frequency of drag coefficients is twice that of the lift coefficients. As can be seen from Fig. 3(a), the frequency of vortex shedding increases with the increase in Re as corroborated by Fig. 2 as well.

5.2 Flows for $3,000 \leq Re \leq 9,500$

Flow around a cylinder at these Reynolds numbers eventually becomes three dimensional and turbulence sets in. Therefore we simulate the flow only for the very early laminar stage and compare our results with those obtained from experiments. At first we compare our numerical results for $Re = 3,000$ with the results of [38] in Table 1. As observed in earlier sections for $Re = 200$ and 550 , a very good agreement of the values of l_{max} and $x_{l_{max}}$ can be found for the early part of flow development. We also compare velocity distributions along the flow axis behind the cylinder for different times with the experimental results of [38] in Fig. 7(b). Next we compare our results with the works of [15] in Fig. 4. From Fig. 4(a) it is seen that the primary vortex behind the cylinder makes its appearance and develops quite early. Shortly afterwards there is the distortion of streamlines somewhere midway between the stagnation and separation points (refer to Fig. 1(c)). Stream lines close to the cylinder deviate from the cylinder causing a bulge pattern, known as bulge phenomenon. As time progresses, this bulge gives rise to a small secondary eddy known as secondary eddy phenomenon which can clearly be seen at time $t = 1.0$ in Fig. 4(b). For $Re = 3,000$, the secondary eddy grows with time, captured in Fig. 4(c), to such an extent that it touches the boundary of the main eddy, thereby splitting the main one into two parts and isolating the region of the wake next to the separation point where another secondary eddy can now be seen. These two secondary eddies are equivalent in size and in strength and constitute pair of secondary eddies. This phenomenon is called α -phenomenon and is distinctly visible in Fig. 4(d). As can be seen from Fig. 4, our computed solutions are excellent match with the experimental ones and closer to them than the numerical results presented in [15].

Next we consider the cases for $Re = 5,000$ and $9,500$. The most important feature of this flow range is that the flow exhibits the so called β phenomenon. In this range, at an early stage, as the back flow near the cylinder starts, a recirculating zone attached to the cylinder is created. As the flow of fluid develops in downstream, due to the high Reynolds number of the flow the core of this recirculating zone gets strengthened quickly. Though the rest of the recirculating zone gathers strength, it is slow compared to its core, thereby setting the stage for the development of secondary vortex. At around $t = 1.0$ this secondary vortex becomes prominent, dividing the primary vortex into two chambers, one of which is the core. Nevertheless the second weaker part maintains some sort of communication with its core part. For some time both the core and the secondary vortex acquire strength and the channel of communication between the two parts of the primary vortex becomes narrow. But as the primary vortex becomes bigger in size again, both its parts starts getting stronger and devour the secondary vortex from left and right, reducing its strength and size. At time around $t = 1.5$ the secondary vortex becomes quite small. This is what is popularly known as β phenomenon. The β phenomena can be clearly seen for $Re = 5,000$ and $9,500$ at times $t = 1.5$ and 1.0 in Figs. 5(a) and 6(a) respectively. For $Re = 5,000$ this β phenomenon quickly leads to the α phenomenon described earlier which can be seen in Fig. 5(b) at time $t = 2.0$ and Fig. 5(c) at $t = 2.5$. But for $Re = 9,500$

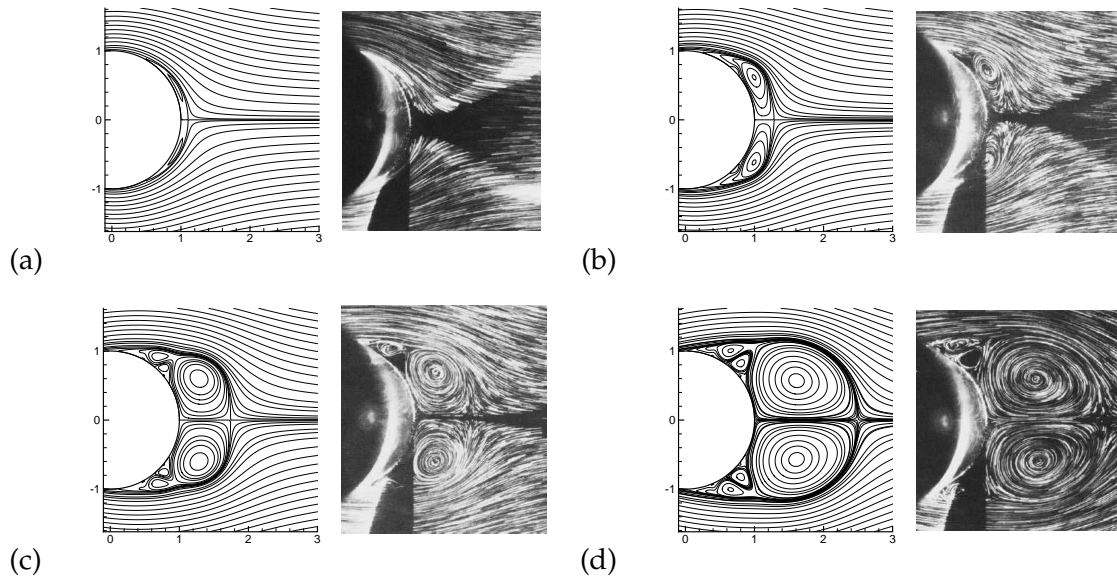


Figure 4: For $Re=3,000$ comparison of numerical and experimental [15] visualization at times (a) $t=0.5$, (b) $t=1.0$, (c) $t=1.5$, (d) $t=2.5$.

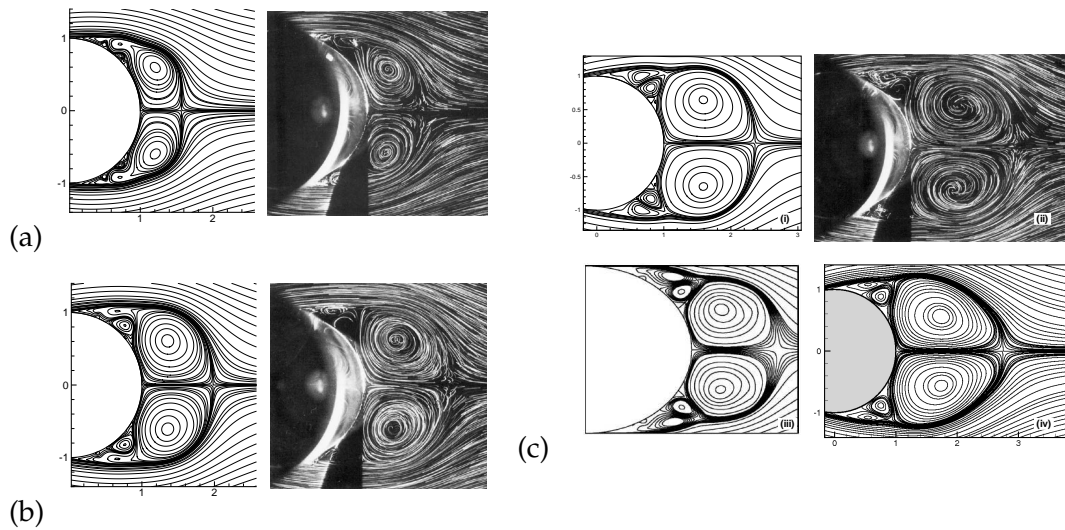


Figure 5: For $Re=5,000$ comparison of numerical and experimental [38] visualizations at time (a) $t=1.5$, (b) $t=2.0$, (c) $t=2.5$. In (c) (iii) is due to Sanyasiraju and Manjula [21]; (iv) is due to Kalita and Ray [22].

the flow becomes unstable later on and α phenomenon cannot be observed (see Figs. 6(b) and 6(c)). Note that in the above mentioned figures we have presented our numerical results side by side with that of experimental results reported in [38]. It is heartening to

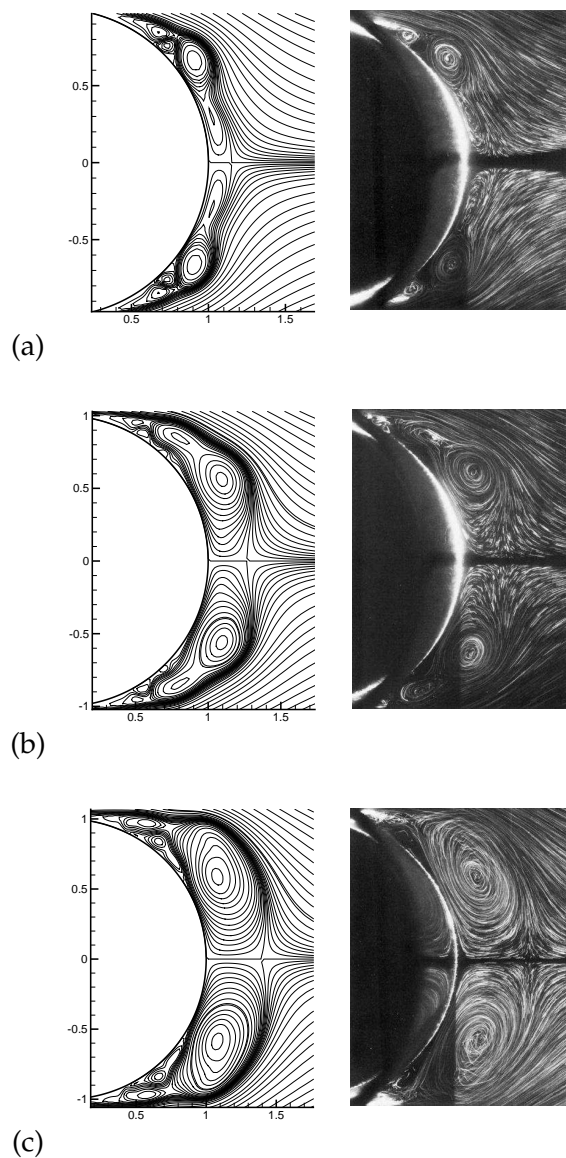


Figure 6: For $Re=9,500$ comparison of numerical and experimental [38] visualizations at time (a) $t=1.0$, (b) $t=1.25$, (c) $t=1.5$.

note that our computed solutions almost exactly replicate the α and β -phenomena of the experimental results of [38] as suggested by Figs. 5 and 6. In Fig. 5(c) we compare our computed results with two other numerical results obtained by Sanyasiraju and Manjula [21] and Kalita and Ray [22] at time $t=2.5$ along side the experimental visualization of [38]. Our computation captures the shape of the primary vortex as also the small sec-

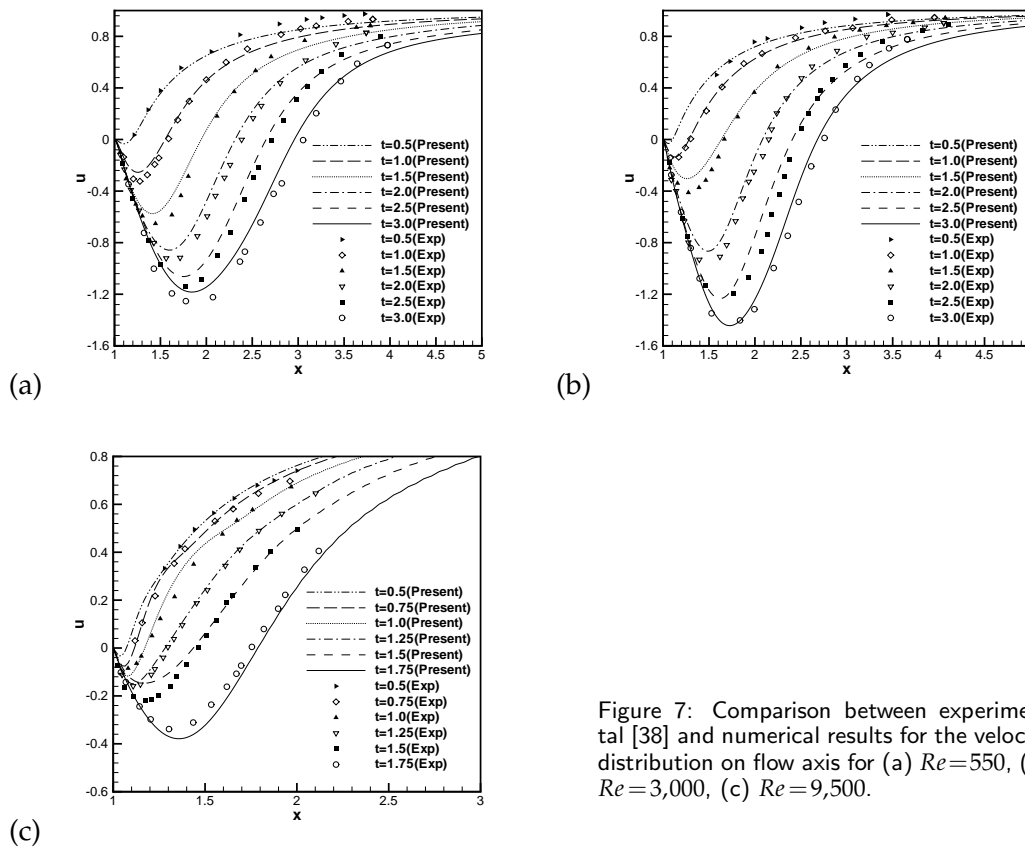


Figure 7: Comparison between experimental [38] and numerical results for the velocity distribution on flow axis for (a) $Re = 550$, (b) $Re = 3,000$, (c) $Re = 9,500$.

ondary vortices most accurately as compared to the other simulations. Fig. 7(c) compares the velocity distribution on the flow axis with the experimental one for $Re = 9,500$. As in the case of $Re = 550$ and $3,000$ a very close comparison is obtained in this case as well.

6 Conclusion

Compact schemes based on biharmonic pure stream function formulation of the transient N-S equations have so far been successfully used only on rectangular cartesian coordinates. In this paper, we carry out a comprehensive numerical validation of the classical problem of the transient flow past an impulsively started circular cylinder by specifically adopting a newly developed implicit scheme for biharmonic form of the Navier-Stokes equation. We have computed the flow for a wide range of Reynolds numbers ranging from 50 to 9,500 and have considered both long time as well as transient cases. In particular, the flow features which are typical of the sub-ranges $50 \leq Re \leq 550$ and $3,000 \leq Re \leq 9,500$ are discussed in details. We compare our results with established ex-

perimental and numerical results, and obtain excellent comparison in all the cases, both qualitatively and quantitatively. The robustness of the scheme is highlighted not only when it captures the periodic nature of the flow for $50 \leq Re \leq 300$, which is characterized by vortex shedding represented by the von Kármán street for which a detailed streakline analysis is provided, but also by the fact that it very accurately captures the so called α - and β -phenomena for higher Re . The strength of the scheme is exemplified by the fact that flow simulations from our computations are much closer to the experimental visualization than other existing numerical simulations available in the literature, particularly for the higher Reynolds numbers. To the best of our knowledge, no pure stream function based scheme for the N-S equations has been employed to simulate the transient flow past a circular cylinder till date. Currently we are working on the extension of the scheme to the oscillating cylinder and cylinder in cross flow problems and preliminary indications are that this would be as successful as its impulsively started circular cylinder counterpart.

Acknowledgments

The first author would like to express his thanks to the DST, India for supporting his research work under Project No. SR/S4/MS: 468/07.

The second author is thankful to the University Grants Commission, India for supporting a part of the work by providing financial support in the form of a minor project (Project No. F. No. 37-537/2009(SR)).

References

- [1] H. Blasius, Grenzschichten in Flüssigkeiten mit kleiner Reibung, *Z. angew. Math. Phys.* 56 (1908) 1-37.
- [2] H. Nisi, A. W. Porter, On eddies in air, *Philosophical Magazine Series 6*, 46 (1923) 754-768.
- [3] S. Goldstein, L. Rosenhead, Boundary layer growth, *Proc. Cad. Phil. Soc.* 32 (1936) 392-401.
- [4] H. Schuh, Calculation of unsteady boundary layers in two dimensional laminar flow, *Z. Fluqwiss* 1 (1953) 122-133.
- [5] E. J. Watson, Boundary layer growth, *Proc. R. Soc. Lond. (A)* 231 (1955) 104-116.
- [6] A. Roshko, On the wake and drag of bluff bodies, *J. Aeronaut. Sci.*, 22 (1955) 124-132.
- [7] S. Taneda, Downstream development of wakes behind cylinders, *J. Phys. Soc. Jpn.* 14 (1959) 843-848.
- [8] D. J. Tritton, Experiments on the flow past a circular cylinder at low Reynolds numbers, *J. Fluid Mech.* 6 (1959) 547-567.
- [9] M. M. Zdravkovich, Smoke observation of the observation of a Karman vortex street, *J. Fluid Mech.* 37 (1969) 491-496.
- [10] D. B. Ingham, Note on the numerical solution for unsteady viscous flow past a circular cylinder, *J. Fluid Mech.* 31 (1968) 815-818.
- [11] P. C. Jain, K. S. Rao, Numerical solution of unsteady viscous incompressible fluid flow past a circular cylinder, *Phys. Fluids Suppl.* 11 (1969) 57-64.

- [12] V. A. Patel, Time dependent solutions of the viscous incompressible flow past a circular cylinder, *Comp. Fluids* 4 (1976) 13-27.
- [13] W. M. Collins, S. C. R. Dennis, Flow past an impulsively started circular cylinder. *J. Fluid Mech.* (1973) 60-105.
- [14] T. P. Loc, Numerical analysis of unsteady secondary vortices generated by an impulsively started circular cylinder, *J. Fluid Mech.* 100 (1980) 111-128.
- [15] T. P. Loc, R. Bouard, Numerical solution of the early stage of the unsteady viscous flow around a circular cylinder: a comparison with experimental visualization and measurements, *J. Fluid Mech.* 160 (1985) 93-117.
- [16] R. Franke, W. Rodi, B. Schonung, Numerical calculation of laminar vortexshedding flow past cylinders. *Journal of Wind Engineering and Industrial Aerodynamics* 35 (1990) 237-257.
- [17] C. H. K. Williamson, Vortex dynamics in the cylinder wake, *Ann. Rev. Fluid Mech.* 28 (1996) 477-539.
- [18] G. K. Batchelor, *An Introduction to Fluid Dynamics*, Cambridge University Press, Cambridge, 2005.
- [19] X. He, G. Doolen, Lattice Boltzmann Method on Curvilinear Coordinates system: Flow around a Circular Cylinder, *J. Comput. Phys.* 134 (1997) 306-315.
- [20] X. D. Niu, Y. T. Chew, C. Shu, Simulation of flows around an impulsively started circular cylinder by Taylor series expansion and least squares-based lattice Boltzmann Method, *J. Comput. Phys.* 188 (2003) 176-193.
- [21] Y. V. S. S. Sanyasiraju, V. Manjula Flow past an impulsively started circular cylinder using a higher-order semicompact scheme, *Phys. Rev. E* 72 (2005) 1-10.
- [22] J. C. Kalita, R. K. Ray, A transformation-free HOC scheme for incompressible viscous flows past an impulsively started circular cylinder, *J. Comput. Phys.* 228 (2009) 5207-5236.
- [23] C. I. Christov, R. S. Marinova, T. T. Marinov, Does the stationary viscous flow around a circular cylinder exist for large Reynolds numbers? A numerical solution via variational imbedding, *J. Comput. Appl. Math.* 226 (2009) 205-207.
- [24] Z.-J. Tan, K. M. Lim, B. C. Khoo, D. S. Wang, An indirect-forcing immersed boundary method for incompressible viscous flows with interfaces on irregular domains, *Commun. Comput. Phys.* 6 (2009) 997-1021.
- [25] Y. Cheng, H. Zhang, C. Liu, Immersed boundary-lattice Boltzmann coupling scheme for fluid-structure interaction with flexible boundary, *Commun. Comput. Phys.* 9 (2011) 1375-1396.
- [26] M. M. Gupta, High accuracy solutions of incompressible Navier-Stokes equations, *J. Comput. Phys.* 93 (1991) 343-359.
- [27] W. F. Spitz, G. F. Carey, Formulation and experiments with high-order compact schemes for nonuniform grids, *Int. J. Numer. Methods Heat and Fluid Flow* 8 (1998) 288-303.
- [28] J. C. Kalita, D. C. Dalal, A. K. Dass, A class of higher order compact schemes for the unsteady two-dimensional convection-diffusion equations with variable convection coefficients, *Int. J. Numer. Methods Fluids* 38 (2002) 1111-1131.
- [29] W. D. Henshaw, A fourth-order accurate method for the incompressible Navier-Stokes equations on overlapping grids, *J. Comput. Phys.* 113 (1994) 13-25.
- [30] W. D. Henshaw, H. O. Kreiss, L. G. M. Reyna, A fourth-order accurate difference approximation for the incompressible Navier-Stokes equations, *Comput. Fluids* 23 (1994) 575-593.
- [31] J. C. Strikwerda, High-order accurate schemes for incompressible viscous flow, *Int. J. Numer. Meth. Fluids* 24 (1997) 715-734.
- [32] A. Bruger, B. Gustafsson, P. Lotstedt, J. Nilsson, High order accurate solution of the

- incompressible NavierStokes equations, *J. Comput. Phys.* 203 (2005) 49-71.
- [33] D. Fishelov, M. Ben-Artzi, J. P. Croisille, A compact scheme for the stream function formulation of Navier-Stokes equations, *Notes on Computer Sciences (Springer-Verlag)* 2667 (2003) 809-817.
- [34] M. Ben-Artzi, J. P. Croisille, D. Fishelov, S. Trachtenberg, A pure-compact scheme for the streamfunction formulation of Navier-Stokes equations. *J. Comput. Phys.* 205 (2005) 640-664.
- [35] M. M. Gupta, J. C. Kalita, A new paradigm for solving NavierStokes equations: streamfunctionvelocity formulation, *J. Comput. Phys.* 207 (2005) 52-68.
- [36] J. C. Kalita, M. M. Gupta, A streamfunction-velocity approach for the 2D transient incompressible viscous flows, *Int. J. Numer. Meth. Fluids* 62 (2010) 237-266.
- [37] J. C. Kalita, S. Sen, Biharmonic computation of the flow past an impulsively started circular cylinder at $Re = 200$, *Lecture Notes in Eng. and Com. Sc.* 2185 (2010) 1805-1810.
- [38] R. Bouard, M. Coutanceau, The early stage of development of the wake behind an impulsively started cylinder for $40 < Re < 10^4$, *J. Fluid Mech.* 101 (1980) 583-607.
- [39] D. Lee, Y. M. Tsuei, A Hybrid Adaptive Gridding Procedure for Recirculating Fluid Flow Problems, *J. Comput. Phys.* 108 (1993) 122-141.
- [40] C. T. Kelly, *Iterative methods for linear and nonlinear equations*, SIAM Publications, Philadelphia, 1995.
- [41] B. Fornberg, A numerical study of steady viscous flow past a circular cylinder, *J. Fluid Mech.* 98 (1980) 819-855.
- [42] V. Dyke, *An Album of Fluid Motion*, The Parabolic Press, California, 1988.